J. Fluid Mech. (1988), *vol.* 196, *pp.* 107–134
Printed in Great Britain

Spreading of the interface at the top of a slightly polydisperse sedimenting suspension

By ROBERT H. DAVIS AND MARK A. HASSEN
Department of Chemical Engineering, University of Colorado, Boulder, CO 80309-0424, USA

(Received 17 July 1987 and in revised form 2 March 1988)

The interface at the top of a dilute sedimenting suspension of small particles which are not identical does not remain sharp but instead becomes increasingly diffuse as the sedimentation proceeds. For more concentrated suspensions, the self-sharpening effect of hindered settling leads to a considerable reduction in the observed spreading of the sedimenting interface. In order to quantify this spreading, a light extinction technique was used to measure the concentration profile in the interface of a suspension of particles with a small spread of sizes as it fell past a thin sheet of light. A particle volume-fraction range of $0.002 \leqslant \Phi_0 \leqslant 0.15$ was examined, and each fluid-particle system had a particle Reynolds number less than 10^{-3} and a Péclet number greater than 10^7 so that inertia and colloidal effects were negligible. Calculations of the spreading arising from the small degree of polydispersity in particle sizes and the self-sharpening effect are presented. Surprisingly, the measured vertical thickness of the interface was found to be several times that predicted from this theory.

It is proposed that the observed spreading may be attributed to hydrodynamic interactions between particles that lead to fluctuations in particle settling velocities about the mean. An analysis of the data shows that the measured interface thickness, after subtracting off that predicted from polydispersity and self-sharpening, increases approximately with the square root of the settling distance and may therefore be described as a diffusion process, termed 'self-induced hydrodynamic diffusion'. By scaling the hydrodynamic diffusivity as $D = au_{\frac{1}{2}}\hat{D}(\Phi_0)$, where $u_{\frac{1}{2}}$ is the median hindered settling velocity, a is the median particle radius, and Φ_0 is the volume fraction of particles well below the interface, an approximate analysis of the data was used to infer that the dimensionless scaled diffusion coefficient, $\hat{D}$, is between 1 and 2 for the smaller particle volume fractions examined, increases very rapidly with increasing concentration to a value between 10 and 15 for particle concentrations of a few percent by volume, and then levels off or declines slightly as the particle concentration is increased further.

1. Introduction

It is well known that the mean rate of sediment of suspended particles with uniform concentration is reduced as their concentration is increased; this observation is commonly referred to as 'hindered settling'. A consequence of hindered settling is the 'self-sharpening effect' by which the spreading of the interface at the top of a sedimenting suspension is reduced as the particle concentration is increased, as illustrated in the educational movie 'Low Reynolds Number Hydrodynamics' narrated by G. I. Taylor. It arises because the particles that are left behind at the top of the interface are in a region of lower concentration than that of the bulk suspension, and they therefore experience diminished hindered settling. Thus, the

difference between the mean hindered-settling velocity of the faster particles at the bottom of the interface and the slower particles at the top of the interface is reduced as the particle concentration is increased, thereby reducing the rate of spreading of the interface.

The observed spreading of the interface is usually attributed to the variation in particle sizes, densities and/or shapes that is present in nearly all suspensions. The vertical thickness of the interface at the top of an initially well-mixed suspension is then expected to increase in proportion to the elapsed time, with the constant of proportionality being a measure of the variation in settling speeds of the particles in the polydisperse suspension.

The motion of a particle sedimenting due to gravity is influenced by the relative positions and velocities of the neighbouring particles. Thus, even in a monodisperse suspension containing spherical particles of identical size and density, the instantaneous velocities of the individual particles vary about the mean sedimentation velocity. For example, the velocity of a particle that forms a close pair with its nearest neighbour is greater than the mean, whereas the velocity of a particle that is relatively isolated from its neighbours is less than the mean. Moreover, since the relative positions of the suspended particles are continually changing, the velocity of each particle fluctuates during the sedimentation process. This behaviour has led to the use of stochastic models for the study of sedimentation, as described by Tory & Pickard (1986). The velocity fluctuations can be shown to lead to particle displacements that can be represented statistically as a diffusion process, termed 'self-induced hydrodynamic diffusion' (G. K. Batchelor, personal communication). The related phenomenon of 'shear-induced hydrodynamic diffusion', in which particles in a sheared suspension undergo migrations about the average streamlines owing to hydrodynamic interactions, has been studied experimentally by Eckstein, Bailey & Shapiro (1977) and by Leighton & Acrivos (1987*a*, *b*), and simulated by Durlofsky, Brady & Bassis (1987).

An important consequence of self-induced hydrodynamic diffusion is that it will contribute to the spreading of the interface at the top of a sedimenting suspension. In contrast to spreading due to particle polydispersity, a purely diffusive spreading of the interface would result in an interface thickness that increases in proportion to the square root of time, similar to that observed in the spreading of a dye front as it flows through a porous medium.

This paper presents a study of the spreading of the interface at the top of a sedimenting suspension of small particles in order to gain insight into the mechanisms that contribute to this spreading. In §2, we present a theory to describe the spreading of the interface for a polydisperse suspension experiencing hindered settling without particle diffusion. The results of this theory for Gaussian size distributions are given in §3 and clearly predict the self-sharpening effect with increasing particle volume fraction. In §4, an experiment is described that measured the degree of interface spreading during the sedimentation of non-Brownian spherical particles with narrow size distributions. The results of these experiments (§5) show that the rate of interface spreading is significantly greater than that predicted for the diffusionless theory. In §6, the data are examined to see whether the additional spreading (in excess of that expected from polydispersity and hindered settling effects alone) could be described as a diffusion process and to infer information on the magnitude of the self-induced hydrodynamic diffusivity.

2. Theoretical description of interface spreading

In this section, a theoretical description of the spreading of the interface at the top of a sedimenting suspension containing a distribution of particle sizes is presented. It is assumed that the sedimentation is described by low-Reynolds-number hydrodynamics, with negligible inertia, Brownian motion and colloidal forces, and that the vessel size is large compared with the particle size. The theory predicts the particle concentration and size distribution as a function of settling depth and time. As depicted in figure 1, these quantities remain equal to their initial values in the bulk suspension below the interface region and above the sediment layer. The total particle concentration decreases in a continuous fashion from the bottom to the top of the interface, as does the average particle size. The interface moves downward with time, and its thickness increases.

Particle concentrations within the interface are governed by the particle-flux continuity equation, supplemented by a hindered-settling relation between sedimentation velocities and local particle concentrations. A continuous distribution of particle sizes may be analysed by solving differential particle-flux continuity equations with finite-difference techniques, as described by Davis, Herbolzheimer & Acrivos (1982). In particular, the differential flux continuity equation is

$$\frac{\mathrm{d}[\phi(U-u)]}{\mathrm{d}U} = \phi. \tag{2.1}$$

Equation (2.1) is derived from a Lagrangian viewpoint by considering a horizontal, isoconcentration slice within the sedimenting interface where $U+\mathrm{d}U$ is the fall speed of the bottom of the slice, U is the fall speed of the top of the slice, and ϕ is the volume fraction within the slice of particles having settling velocity u. The left-hand side of (1.1), when multiplied by $\mathrm{d}U$, is the difference between the rate at which particles with settling velocity u enter the bottom of the slice and that at which they exit the top of the slice, and the right-hand side represents their rate of accumulation within the slice whose thickness increases at a rate $\mathrm{d}U$. Equation (2.1) holds for all $u < U$ and for all U between the minimum (top) and maximum (bottom) fall speeds of isoconcentration planes within the sedimenting interface.

In the present paper, we choose instead to follow the development of Smith (1966) and first discretize the continuous distribution and then to use a particle flux continuity equation for each discrete particle species. As will be shown, this is equivalent to choosing a particular finite-difference scheme for solving (2.1). A continuous distribution of particle sizes is modelled by dividing the total size range into N intervals. The value of N is chosen to be sufficiently large that it does not significantly influence the final results. Each interval is represented by its midpoint diameter and has a concentration equal to the total particle concentration multiplied by the fractional probability for the interval in question, which is equal to the area under the continuous probability density function between the lower and upper diameters defining the interval. As described by Davis & Acrivos (1985), and depicted in figure 1, the interior of an initially well-mixed suspension of N discrete particle species will stratify into N layers. The lowest layer (layer 1) represents the bulk suspension and contains all N species of particles at their original concentrations. Above this is layer 2, which is devoid of the fastest-settling species. Each successive layer is devoid of the fastest-settling species from the layer below; the top layer (layer N) contains only the slowest-settling particle species, and above it is a growing clarified fluid layer. Of course, beneath layer 1 is a growing sediment layer

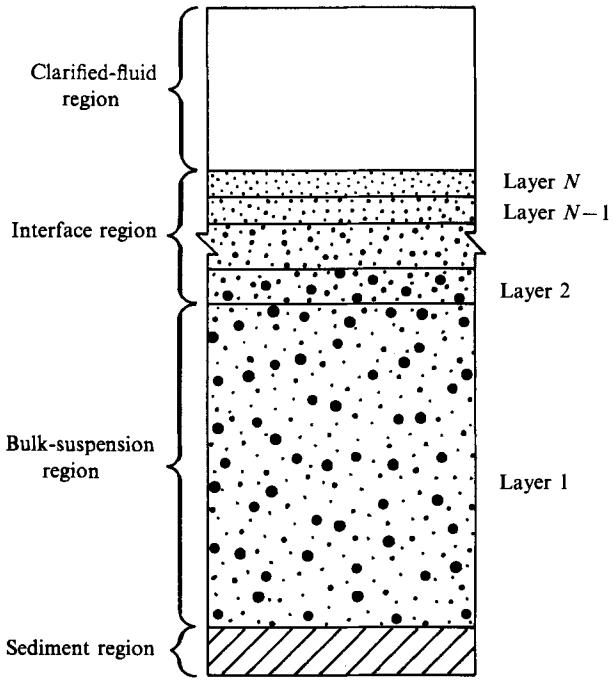

FIGURE 1. Schematic of the sedimentation of a discretized polydisperse suspension.

of stationary particles. The fan of thin layers from layer 2 up to layer N represents the expanding interface. Our goal is to determine the particle concentrations and velocities in each of these layers and then to use this information to predict useful macroscopic information such as the rate of spreading of the interface. Note that the distribution of particles is uniform in any horizontal plane. No lateral segregation is expected, in agreement with the theory of Batchelor & Janse van Rensburg (1986) which shows that suspensions of equidensity particles are stable.

2.1. *Particle-flux continuity equation*

The particle-flux continuity equation for multispecies sedimentation was first developed by Smith (1966) and has subsequently been used by several investigators to study the sedimentation of polydisperse suspensions, as reviewed by Davis & Acrivos (1985). This equation is given by

$$\phi_{i,k+1}(u_{kk}-u_{i,k+1}) = \phi_{ik}(u_{kk}-u_{ik}); \quad i = k+1,\ldots,N \tag{2.2}$$

and represents a jump condition for the concentration of particle species i when moving from layer k to layer $k+1$. The left-hand side is the rate at which particles of species i enter the bottom of layer $k+1$, and the right-hand side is the rate at which they leave the top of layer k. These must be equal in order to satisfy mass conservation at the shock surface separating layers k and $k+1$. The particle species are numbered successively so that species k is the fastest-settling particle in layer k. In (2.2), the first subscript refers to the particle species, and the second subscript refers to the layer within the interface; thus, ϕ_{ik} is the volume fraction of species i in layer k, and u_{ik} is the average sedimentation velocity of species i in layer k. We note that (2.2) may also be derived by integrating (2.1) from the top of layer $k(U = u_{kk})$ to the top of layer $k+1(U = u_{k+1,k+1})$. Thus, using (2.2) is equivalent to solving

(2.1) by a first-order Euler's finite-difference method, only with ϕ on the right-hand side of (2.1) being evaluated at the end of the step ($\phi = \phi_{i,k+1}$) rather than at the beginning of the step ($\phi = \phi_{ik}$). Equation (2.2) is supplemented by the constraint that species k is only present in layer k and below, i.e.

$$\phi_{i,k+1} = 0; \quad i = 1, \ldots, k. \tag{2.3}$$

Finally, we note that only the flux of particles due to their mean sedimentation velocities is included in (2.2). In situations where Brownian diffusion or self-induced hydrodynamic diffusion of particles are significant, the rate of spreading of the interface will be higher than that predicted by this theory, as will be shown by the experimental results presented in §5.

2.2. *Hindered-settling functions*

Equation (2.2) cannot be solved for both the volume fraction and the settling velocity of each particle species in each layer. The required additional information is a hindered-settling function, which relates the settling velocity of each particle species to the local concentrations of all of the particles present:

$$u_{ik} = u_{i,0} f_{ik}, \tag{2.4}$$

where f_{ik} is the hindered-settling function for particle species i in layer k, and $u_{i,0}$ is the terminal settling velocity for an isolated particle of species i. For spherical particles of radius a_i and density ρ_i falling through a Newtonian fluid of viscosity μ and density ρ at small particle Reynolds number, $u_{i,0}$ is given by Stokes law:

$$u_{i,0} = 2a_i^2(\rho_i - \rho)\, g/9\mu, \tag{2.5}$$

where g is the acceleration constant.

The hindered-settling function f_{ik} in general will depend on the volume fractions of all of the species present in layer k. In supposing that the hindered functions depend only on the local volume fractions, an assumption is made that the volume fractions vary in the vertical direction over a lengthscale that is large compared with the particle size so that the suspension behaves locally like a homogeneous dispersion. This will be true after a short transient period. In a dilute dispersion the hindered-settling function is of the form

$$f_{ik} = 1 + \sum_{j=k}^{N} S_{ij}\, \phi_{jk}. \tag{2.6}$$

Batchelor (1982) has derived formulae for the dimensionless sedimentation coefficients S_{ij}, and they have been calculated numerically by Batchelor & Wen (1982) as functions of the size ratio a_j/a_i and the reduced density ratio $(\rho_j - \rho)/(\rho_i - \rho)$. Equation (2.6) is based upon a pairwise theory of particle interactions and is restricted to dilute suspensions for which the total particle volume fraction is less than about 0.05. In experiments with dilute bidisperse and tridisperse experiments, Davis & Birdsell (1988) found very good agreement with predictions using (2.6) and the appropriate sedimentation coefficients calculated by Batchelor & Wen (1982). For equidensity spheres, the sedimentation coefficients are always negative. When the ratio a_k/a_i is very large, (2.6) may yield negative values for f_{ik}, indicating that small particles may move upwards owing to the upswelling of the suspending fluid caused by the sedimentation of large particles (Greenspan & Ungarish 1982). For the narrow size distributions of particles used in experiments described in this paper, this effect is not predicted, nor was it observed.

Since only limited sedimentation data for polydisperse suspensions are available, hindered settling functions based upon the results for monodisperse suspensions are often adapted for polydisperse suspensions. A widely used formula of this type is based upon the Richardson & Zaki (1954) correlation for a monodispersion, viz.

$$f_{ik} = (1-\Phi_k)^n, \tag{2.7}$$

where

$$\Phi_k \equiv \sum_{j=k}^{N} \phi_{jk} \tag{2.8}$$

is the total volume fraction of particles in layer k, and the exponent n is generally assigned a value of approximately 5 in order to represent most accurately the data for low Reynolds numbers. Another common monodisperse formula is that presented by Barnea & Mizrahi (1973):

$$f_{ik} = \frac{(1-\Phi_k)^2}{(1+(\Phi_k)^{\frac{1}{3}}) \exp(5\Phi_k/3(1-\Phi_k))}. \tag{2.9}$$

Because of the simplicity and accuracy of the Richardson–Zaki correlation in representing settling data over a wide range of particle volume fraction, (2.7) will be used for the calculations presented in this paper, unless otherwise noted. An exponent of $n = 5.0$ is chosen for use in (2.7) based upon the findings obtained by Davis & Birdsell (1988) for sedimentation of particles with narrow size distributions. Since we restrict our attention in this work to relatively narrow size distributions, it is expected that a hindered-settling function that depends only on the total local particle concentration should be adequate. The validity of this approximation is discussed further in §5.

2.3. *Method of solution*

Substituting (2.4) into (2.2) yields

$$\phi_{i,k+1}(u_{k,0}f_{kk} - u_{i,0}f_{i,k+1}) = \phi_{ik}(u_{k,0}f_{kk} - u_{i,0}f_{ik}) \tag{2.10}$$

for all $k = 1, \ldots, N-1$ and for $i = k+1, \ldots, N$. Since $f_{i,k+1}$ is a function of the volume fractions of the particle species present in layer $k+1$, (2.10) represents a system of $N-k$ coupled nonlinear algebraic equations for the particle volume fractions in layer $k+1$. The solution of these equations requires that the species volume fractions in layer k are known. Thus, we start at the lowest region of the suspension (layer 1) where the volume fraction of each particle species is at its specified initial value. Equation (2.10) with $k = 1$ is then solved for the particle concentrations in layer 2, except that (2.3) is also used to give $\phi_{1,2} = 0$. In a similar manner, the calculation is propagated up through the fan of layers to the top of the interface. The velocity of each particle species in each layer is related to the volume fractions through (2.4) and the chosen hindered settling function.

The solution of (2.10) for each successive layer was performed using a nonlinear, unconstrained minimization technique. Squaring (2.10) and summing over all particle species gives the required minimization function for layer $k+1$:

$$F_{k+1} = \sum_{i=k+1}^{N} [\phi_{i,k+1}(u_{k,0}f_{kk} - u_{i,0}f_{i,k+1}) - \phi_{ik}(u_{k,0}f_{kk} - u_{i,0}f_{ik})]^2. \tag{2.11}$$

An effective algorithm for minimizing F_{k+1} was provided by R. B. Schnabel and L. Flach (personal communication). In this algorithm, a secant technique is used to compute a Hessian matrix for a 'quasi-Newton' search for the vector of solutions

giving a minimum value to the supplied function. An important restriction placed on the function to be minimized is that the solution-vector components should be of similar magnitude. Since species concentrations in a layer within the sedimenting interface may easily span several orders of magnitude, each concentration must be scaled before use of the algorithm. Scaling factors were obtained from the initial distribution and then updated for each consecutive layer. Also, the isolated sedimentation velocities in (2.11) were non-dimensionalized using the Stokes velocity of the median particle size. The minimization technique yielded a value of zero (within the specified relative accuracy of 10^{-4}) for each term in the summation in (2.11).

3. Numerical results and discussion

We restrict our attention to equidensity particles whose sizes have a normal or Gaussian distribution about the mean on a volume basis. The theoretical predictions for particle concentrations and velocities in the sedimenting interface then, in dimensionless form, depend on two dimensionless parameters: Φ_0, the total initial volume fraction, and σ/a, the relative spread in the size distribution, where a is the mean particle radius and σ is the standard deviation in particle radii about the mean. A total radius range of 4 standard deviations above and below the median was used in the numerical calculations. This range was subdivided into N discrete particle species. The value of N was varied from $N = 10$ to $N = 30$. It was found that a value of $N = 25$ gave particle concentration distributions that had converged with a relative error of less than 10^{-3} for all cases examined.

Figure 2 shows typical solutions to (2.11) for $\Phi_0 = 0.02$ and 0.05, and $\sigma/a = 0.057$ (based upon one of the particle distributions used in the experiment, with $a = 70$ μm and $\sigma = 4$ μm). Plotted is the volume fraction of each species for each layer versus the corresponding radius. Thus, the curve labelled $k = 1$ gives the species volume fractions in layer 1 and shows the initial Gaussian size distribution, whereas the curve labelled $k = 13$, for example, gives the species volume fractions in layer 13, which is devoid of the 12 fastest-settling species of particles. These results give the particle size distributions and concentrations in each layer in the interface region. In order to achieve the goal of predicting these quantities as a function of settling depth and time, the location of each layer is needed as a function of time. These are easily determined. Once the species volume fractions ϕ_{ik} are found, then the corresponding hindered-settling velocities u_{ik} may be found from (2.4)–(2.9). The rate of fall of the interface separating region k from region $k+1$ above is equal to the fall velocity of the largest particles in region k, u_{kk}. Thus, region k is located between $z = (u_{k-1,k-1})t$ and $z = u_{kk}t$ after a settling time t, where z is measured downward from the top of the liquid.

3.1. *Interface median velocity*

An important piece of information that may be obtained from the solution is the predicted rate of fall of the interface. Since the interface spreads as the sediment proceeds, the rate of fall does not have a unique value. For reasons discussed later, we chose to examine the rate of fall of the location within the interface where the total particle volume fraction, Φ, is equal to one-half of the particle volume fraction in the bulk suspension. This rate of fall is termed the interface median velocity and denoted by $u_{\frac{1}{2}}$. It is found by first identifying the layer k within the interface where $\Phi_k = \frac{1}{2}\Phi_0$. The interface median velocity is then the fall velocity of the top of that

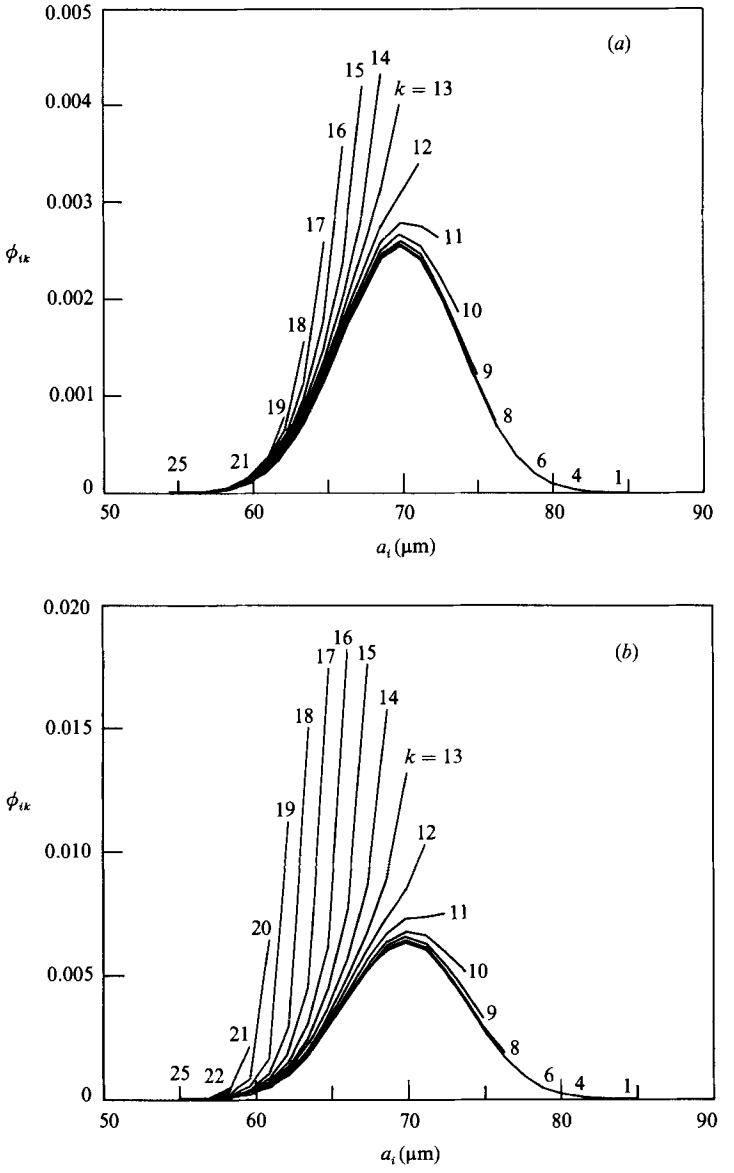

FIGURE 2. Particle species concentrations in the 25 layers of a polydisperse suspension with an initial Gaussian size distribution, having $\sigma/a = 0.057$ and (*a*) $\Phi_0 = 0.02$, (*b*) $\Phi_0 = 0.05$, approximated by dividing it into 25 discrete particle species. The median particle radius is chosen to be $a = 70$ μm.

layer, $u_{\frac{1}{2}} = u_{kk}$. An interpolation procedure is used if the total particle volume fractions of two adjacent layers bracket $\frac{1}{2}\Phi_0$.

In figure 3, the interface median velocity is made dimensionless with the Stokes velocity of the median particle size, $u_{\frac{1}{2},0}$ and plotted versus Φ_0. Also shown as the dashed line in figure 3 is the Richardson–Zaki hindered settling function (2.7) with Φ_k replaced by Φ_0. This coincides within 1.5%, for all Φ_0, with the solid line, which was computed from the complete polydisperse solution of (2.11) for $\sigma/a = 0.057$. Note that the values for the hindered-settling function required in (2.11) were also

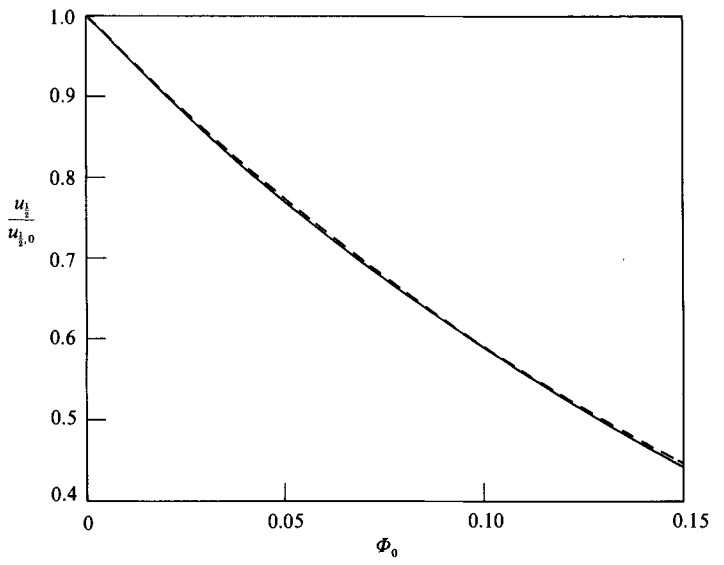

FIGURE 3. The effect of self-sharpening on the interface median velocity. The solid line is the prediction of the polydisperse theory, and the dashed line is the hindered-settling prediction for a monodisperse suspension with all particles having the median size.

obtained from (2.7). Results for other values of σ/a up to 0.25 (the largest relative spread investigated) were also found to agree with the dashed line within 2%. This was also the case when (2.9) was used instead of (2.7) in both the polydisperse and monodisperse calculations.

The findings above lead to the very important conclusion that the speed of movement of the isoconcentration plane were $\Phi/\Phi_0 = \frac{1}{2}$ for a narrowly distributed polydisperse suspension is nearly identical to the hindered settling velocity at the same total particle concentration Φ_0 of a monodisperse suspension with all particles equal in size to the median particle size in the polydisperse suspension. This conclusion may appear paradoxical because the hindered-settling effect is weaker in the polydisperse suspension at the location where $\Phi = \frac{1}{2}\Phi_0$ than in the monodisperse suspension where $\Phi = \Phi_0$. The resolution comes from the particle flux continuity requirement which causes the largest particle size present in the layer where $\Phi = \frac{1}{2}\Phi_0$ in the polydisperse suspension to become progressively smaller than the median size in the bulk suspension as Φ_0 is increased. This behaviour is implied in figure 2 where it is seen that the largest particle radius is less than the median radius of 70 μm for the layer where the area under the curve is one-half that of the bulk suspension (layer 1). For $\Phi_0 = 0.02$, this is layer 15, and for $\Phi_0 = 0.05$, this is layer 17.

3.2. *Rate of spreading of the interface*

In the previous section, the solution of (2.11) was used to determine the fall velocity of the isoconcentration plane within the interface where $\Phi/\Phi_0 = \frac{1}{2}$. In a similar manner, the velocity of other isoconcentration planes may be determined. In figure 4, these velocities are plotted versus the total local solids volume fraction for three Gaussian particle size distributions. The vertical displacement of all three curves from unity at $\Phi/\Phi_0 = \frac{1}{2}$ is a result of hindered settling. Also, the dimensionless velocities of the isoconcentration planes within the spreading interfaces for the three suspensions are nearly equal for $\Phi/\Phi_0 = \frac{1}{2}$, but they diverge away from this point. As

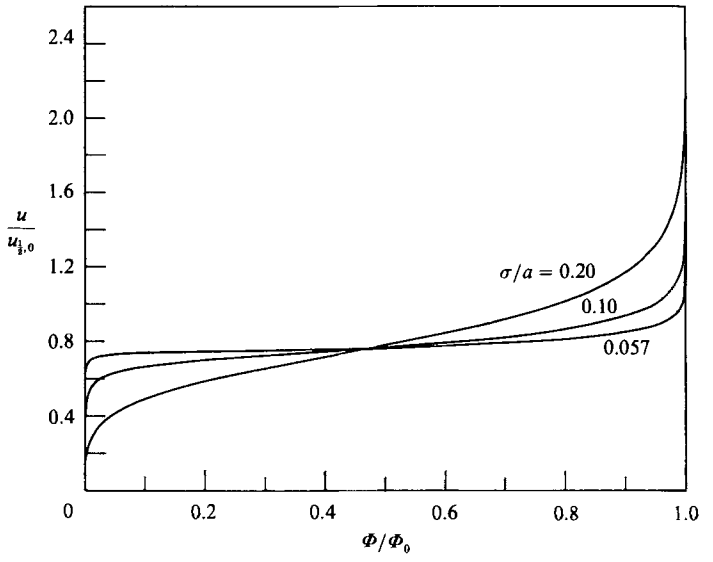

FIGURE 4. The influence of the particle size distribution on the spread of isoconcentration fall velocities of the interface for $\Phi_0 = 0.05$.

expected, the most narrow size distribution gives a relatively sharp velocity profile within the interface, whereas the broader size distributions give broader spreads in settling velocities.

Of more interest for the present purposes is the effect of increasing concentration on the interface for a single size distribution. This is shown in figure 5 where the dimensionless isoconcentration velocities are plotted for $\sigma/a = 0.057$ and $\Phi_0 = 0$, 0.05, and 0.10. The consequences of hindered settling are clearly evident from this figure. First, the interface falls more slowly as Φ_0 is increased. Second, the self-sharpening effect becomes more pronounced as Φ_0 is increased. In the dilute limit ($\Phi_0 \to 0$), the shape of the curve is given directly from the Gaussian size distribution and the size-dependence of the Stokes settling velocities. For $\Phi_0 = 0.10$, the velocity profile is very flat, indicating that the particles within the interface fall with only a small spread in velocities, and so the interface remains relatively sharp.

In the absence of a diffusive spreading mechanism, the thickness of the interface at the top of a sedimenting suspension increases in proportion to the settling time, with the constant of proportionality being a measure of the spread in settling velocities of the particles within the interface. Since there is a continuous spreading velocities for a continuous distribution of particles sizes, a choice must be made in order to define a unique interface thickness. A convenient definition is the quartile interface thickness defined as

$$\delta_p(t) = (u_{\frac{3}{4}} - u_{\frac{1}{4}})\, t, \tag{3.1}$$

where $\delta_p(t)$ is the quartile thickness of the interface after batch settling of an initially well-mixed suspension in a vertical vessel for a time t, and $u_{\frac{1}{4}}$ and $u_{\frac{3}{4}}$ are the velocities of the isoconcentration planes within the interface where $\Phi/\Phi_0 = \frac{1}{4}$ and $\frac{3}{4}$, respectively. The subscript p is included to emphasize that this interface thickness is from the effects of polydispersity and hindered settling alone; diffusion is not

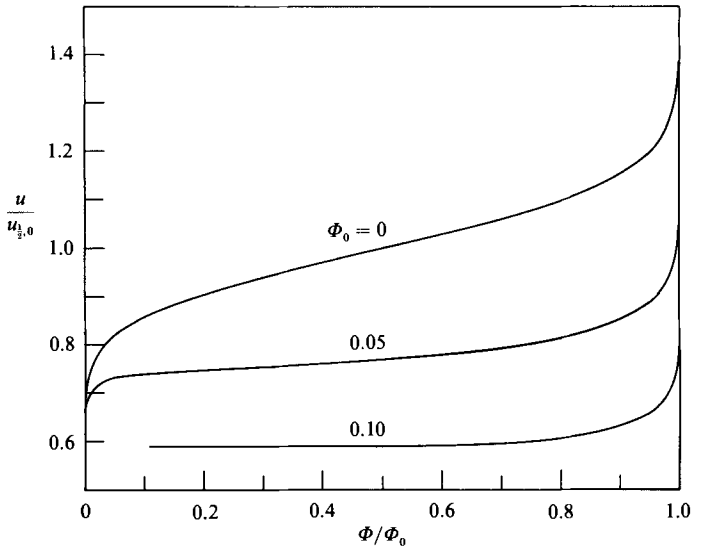

FIGURE 5. The self-sharpening effect of particle concentration on the spread of isoconcentration fall velocities of the interface for $\sigma/a = 0.057$.

included in this prediction. By defining a sedimentation distance as $h = u_{\frac{1}{2}}t$, (3.1) may be recast to give a dimensionless or relative quartile interface thickness:

$$\frac{\delta_p}{h} = \frac{u_{\frac{3}{4}} - u_{\frac{1}{4}}}{u_{\frac{1}{2}}}. \tag{3.2}$$

The velocity difference $u_{\frac{3}{4}} - u_{\frac{1}{4}}$ is the time rate of increase of the thickness of the sedimenting interface. From figures 4 and 5, it is seen that this decreases as σ/a decreases (more narrow distributions) or as Φ_0 increases (the self-sharpening effect). These trends are quantified in figure 6 where the relative quartile interface thickness is plotted as a function of the total initial particle volume fraction for different values of the relative standard deviation in particle sizes. The relative quartile interface thickness in the limit $\Phi_0 \to 0$ may be determined directly from the initial size distribution. In this limit, the particles settle according to (2.4) so that (3.2) becomes

$$\frac{\delta_p}{h} = \frac{a_{\frac{3}{4}}^2 - a_{\frac{1}{4}}^2}{a^2}, \tag{3.3}$$

where, for a Gaussian distribution with median radius a and standard deviation σ, the first and third quartile radii are, respectively $a_{\frac{1}{4}} = a - 0.67\sigma$ and $a_{\frac{3}{4}} = a + 0.67\sigma$. Substituting these values into (3.3) gives

$$\frac{\delta_p}{h} = \frac{2.70\sigma}{a}, \tag{3.4}$$

indicating that the relative interface thickness increases in proportion to the relative standard deviation in particle sizes, in the dilute limit.

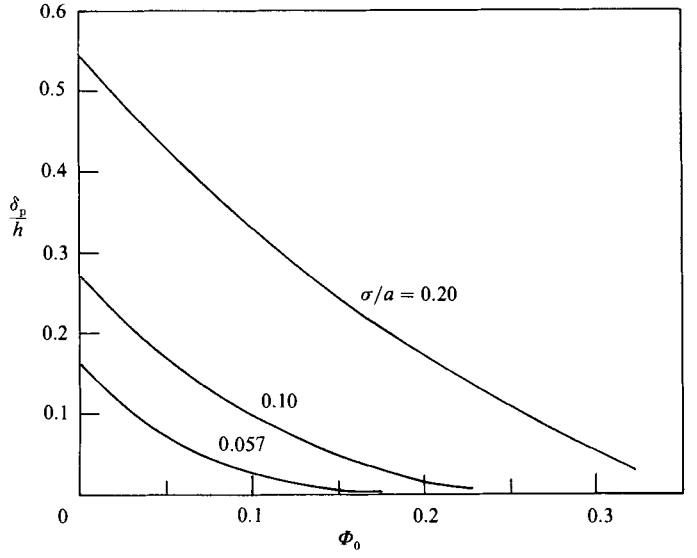

FIGURE 6. Relative quartile interface thickness variation with total particle volume fraction for $\sigma/a = 0.057$, 0.10, and 0.20.

3.3. *Concentration buildup in upper layers of the interface*

Referring back to the 'porcupine' shape in figure 2, it is noted that although the total particle concentration in any given layer is lower than that in the layer below, the concentration of each individual species is higher than in the layer below. This is possible because the upper layer contains one less particle species. These findings may be expressed as

$$\Phi_{k+1} < \Phi_k, \quad k = 1, 2, \ldots, N-1, \tag{3.5}$$

$$\phi_{i,k+1} > \phi_{ik}, \quad i = k+1, \ldots, N. \tag{3.6}$$

The validity of (3.5) and (3.6) is easily proved from (2.10) for the usual case of a hindered-settling function that decreases monotonically with increasing total solids volume fraction.

An interesting physical situation arises when the volume fraction is made sufficiently high that the hindered-settling velocity of the fastest-settling particles in the bulk suspension is reduced below the isolated fall velocity of the slowest-settling particles. In this situation, one might expect that a steady, sharply defined interface would develop because the slower-settling particles would tend to catch back up to the bulk suspension if they were left behind at the top of the interface in a region of very low concentration. This is not the case, however, because the particle volume fraction at the very top of the interface increases as Φ_0 is increased so as to ensure that the slowest-settling particles at the top of the interface fall slower than the fastest-settling particles at the bottom of the interface.

This is illustrated for a variety of size distributions in figure 7 where the relative volume fraction in the top layer of the interface, Φ_N/Φ_0, is plotted versus Φ_0 for $\sigma/a = 0.057$, 0.081, and 0.15. It is seen that the concentration at the top of the suspension is near zero for Φ_0 less than a critical value that increases with the breadth of the size distribution (for Φ_0 less than the critical value, Φ_N/Φ_0 approaches zero in the limit as N becomes large). Above the critical value of Φ_0, the concentration at the top of the suspension has a non-zero value that increases with increasing Φ_0. The

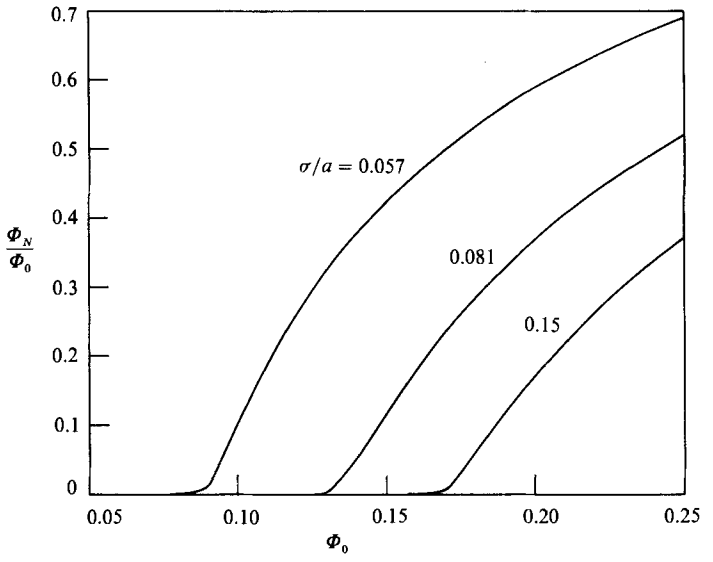

FIGURE 7. The variation of the particle volume fraction of the upper layer in the interface with total initial particle volume fraction for $\sigma/a = 0.057$, 0.081, and 0.15.

critical value of Φ_0 must be larger than the volume fraction at which the hindered-settling velocity of the larger particles is equal to the isolated-settling velocity of the smaller particles so as to assure that hindered settling causes the top of the interface to fall more slowly than the bottom of the interface. Finally, we note that the predicted results in figures 3–7 do not change significantly when N is increased from the value used ($N = 25$).

4. Experiment: materials and methods

An experimental study was carried out in our laboratory in order to quantify the degree of spreading of the interface at the top of a sedimenting suspension by using a light-extinction technique to measure the concentration profile in the interface as it fell past a thin horizontal sheet of light. Details of the experimental apparatus, materials, and methods are given in the thesis by Hassen (1987) and are summarized here.

4.1. *Particles and fluids*

The experiments were carried out in a single Newtonian fluid with two types of spherical glass beads. Particles of type 1 were Class V microbeads (Ferro Corporation) which were supplied presieved between US standard sieve numbers 100 and 120 (having openings of 149 and 125 microns, respectively). These beads were further sieved in order to reduce the fraction of beads that were smaller than the smaller sieve openings. The particle size distribution was analysed by microphotography, sedimentation and conductivity measurement, and was found to be approximately Gaussian with a median particle radius of $a = 70$ μm and a standard deviation of $\sigma = 4$ μm (by volume). Particles of type 2 were Class IV microbeads (Ferro Corporation) which were supplied presieved between US standard sieve numbers 100 and 140 (the latter having openings of 105 microns). They were found also to have Gaussian distribution, with a median radius of $a = 61$ μm and a standard deviation

of $\sigma = 6$ μm. The particle densities were determined by measuring with a hydrometer the density of a liquid in which the particles were neutrally buoyant. For each particle type, the solid density is $\rho_s = 2.49\,\mathrm{g/cm^3}$. A small (less than 1%) variation in particle densities was observed owing to the presence of small air bubbles inside the particles. The suspending fluid was a blend of 49% by mass UCON 50-HB-280X (Union Carbide) and 51% Monsanto HB-40, with the blend composition chosen so as to match closely the refractive index of the glass beads. The measured properties of this fluid at 25.0 °C are a viscosity of $\mu = 85$ cP, a density of $\rho = 1.016\,\mathrm{g/cm^3}$, and a refractive index of 1.518.

4.2. *Experimental procedure*

All of the experiments were carried out in a vertical rectangular vessel with glass walls and having inside dimensions of 40 cm high and 5.1 cm by 3.3 cm in cross-section. Experiments were carried out by introducing weighed amounts of fluid and particles into the vessel which was immersed in a glass-walled water bath controlled at a temperature of 25.0 °C. The volume fractions of the particles in the experiments were varied throughout the range $0.002 < \Phi_0 < 0.15$. After allowing the system to reach thermal equilibrium, a plunger was used to mix the suspension. The plunger was moved vigorously up and down and back and forth through the suspension for several minutes in order to remove as far as possible any initial inhomogeneities in the suspension; care was taken, however, to not entrain any air bubbles through the liquid/air interface. At the cessation of stirring, a clock was started to mark the beginning of sedimentation. Residual motion from the stirring was damped out by the suspension viscosity in less than a few seconds. However, vertical convective motions on lengthscales much greater than the particle spacing were sometimes observed visually in the interior of the suspension, presumably due to slight macroscopic inhomogeneities in the particle concentration, such as would be expected from statistical considerations of random placements of the particles in the suspension. When such motions were observed, the experiment was stopped and the suspension was stirred further prior to restarting. Fortunately, these buoyancy-driven convective motions in the interior rapidly turned over so that the suspension became quiescent, and they did not appear to affect the stably stratified interface at the top of the suspension.

The sedimenting suspension was analysed using a light-extinction principle similar to that employed by the Sedigraph 5000D Particle Sizer Analyzer produced by Micromeritics. The suspension sedimented past a thin horizontal sheet of light (1.0 cm wide by 0.06 cm high) produced by passing a 2 mW He–Ne laser beam (Uniphase Corporation) through a set of cylindrical lenses (Melles-Griot). The light transmitted through the vessel was focused onto a photodiode, and the voltage signal proportional to the transmitted light intensity was recorded as a function of time through an analog-to-digital converter into a microcomputer and stored for later smoothing and analysis, as described by Hassen (1987). As shown in figure 8, two light beams were used simultaneously, one below the other in order to acquire two measurements of the interface per sedimentation run. For each suspension, the experiments were repeated so that typically four to six measurements of the interface were made for each value of h (where h is the vertical distance of the light slit below the liquid/air interface), and four different values of h were examined: $h = 1.5$, 6.0, 24 and 32 cm.

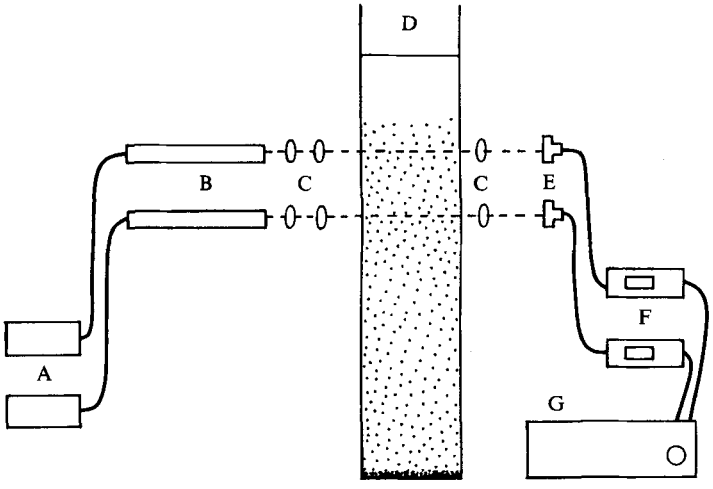

FIGURE 8. The sedimentation/light-extinction apparatus: A, power supplies; B, lasers; C, cylindrical converging and diverging lenses; D, vessel containing the suspensions; E, photodiodes; F, power meters; G, microcomputer.

4.3. *Method of analysis of light-intensity data*

Except for noise, which we have analysed to show that it arises from the statistical fluctuation of the number of particles in the beam at any instant (and which may be removed digitally), $I(t)$ has a very simple, sigmoidal shape, as illustrated in figure 9. At time $t = 0$, the beam passes through the initially well-mixed suspension of volume fraction Φ_0, and a constant intensity I_0 is observed from $t = 0$ to $t = t_0$. At time t_0, the last of the fastest particles in the suspension fall past the beam, and the intensity begins to rise as the concentration in the beam decreases. As the rest of the interface falls past the beam, the amount of light transmitted through the suspension increases until $t = t_f$, at which time all the particles have fallen past the beam, and a constant intensity I_f is recorded, coinciding with the beam's passage through clear fluid above the interface.

Each point of $I(t)$ corresponds to a total solids volume fraction $\Phi(t)$ in the suspension. We use a modified form of Beer's law to relate the light absorbed by the suspension to the concentration of particles. The relationship is derived by supposing that the light absorbance is proportional to the total cross-sectional area of particles present in the beam (Herdan 1960), and is stated as

$$A(t) = \log_{10}\left[\frac{I_f}{I(t)}\right] = k\frac{\Phi(t)}{a^*(t)}, \tag{4.1}$$

where k is a proportionality constant, $\Phi(t)$ is the volume fraction of particles in the beam at time t, and $a^*(t)$ is the area-averaged radius of particles in the beam. This relationship is valid only if the particle volume fraction is sufficiently low that multiple scattering effects are negligible. Calibrations by Davis & Birdsell (1988) with suspensions similar to those used in this work indicate that the range of validity is only $\Phi \leqslant 0.02$ when the refractive indices of the particles and fluid are not matched, whereas this is extended to $\Phi \leqslant 0.15$ when the refractive indices are matched as closely as possible (note that an exact match is not possible owing to the presence of

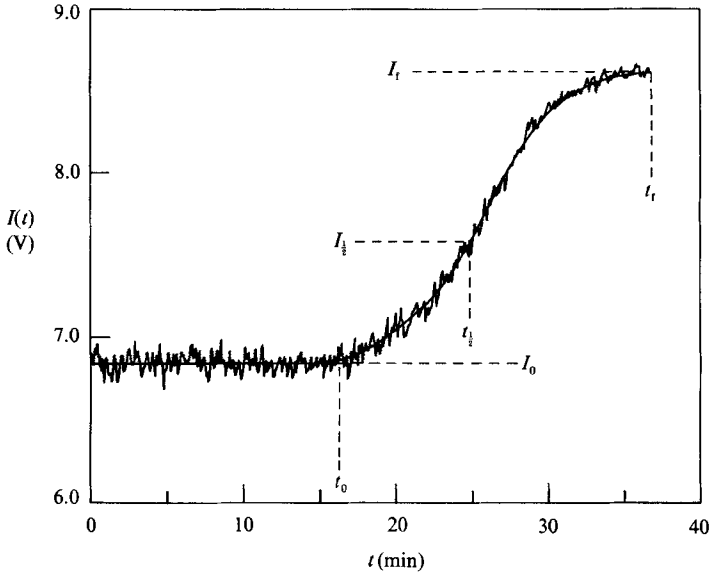

FIGURE 9. Typical raw and smoothed transmitted light intensity versus time data.

the small air bubbles in the particles). Equation (4.1) may be used to define a parameter x:

$$x = \frac{\Phi(t)}{\Phi_0}\frac{a_0^*}{a^*(t)} = \frac{\log_{10}[I_f/I(t)]}{\log_{10}[I_f/I_0]}, \tag{4.2}$$

where a_0^* is the area-averaged particle radius in the initial suspension. Equation (4.2) may be solved for $I(t)$ to yield

$$I(t) = I_0^x I_f^{1-x}. \tag{4.3}$$

Equation (4.3) is the primary working relationship for analysing the data because it specifies the transmitted light intensity corresponding to any given particle volume fraction within the interface. For example, in figure 9 is shown the value of $I(t) = I_{\frac{1}{2}}$ as calculated from (4.3) with $\Phi = \frac{1}{2}\Phi_0$. The corresponding settling time at which the particle volume fraction in the beam is $\frac{1}{2}\Phi_0$ is denoted by $t_{\frac{1}{2}}$, which is equal to the value of the abscissa of the light intensity versus time curve when the ordinate has a value of $I_{\frac{1}{2}}$, as shown in figure 9.

The ratio a_0^*/a^* represents a 'correction' to Beer's law for the presence of polydispersity in the suspension. Observe that for a monodisperse suspension, a_0^*/a^* is unity. For a slightly polydisperse suspension, this ratio remains close to unity, but for highly polydisperse suspensions, the ratio a_0^*/a^* can become significantly greater than unity (note that $a^*(t) < a_0^*$ for $t > t_0$ because the largest particles are then no longer present in the beam). For dilute polydisperse suspensions in which hindered settling is negligible, a_0^*/a^* may be computed iteratively from the light-intensity data $I(t)$, as demonstrated in the thesis of Hassen (1987). For non-dilute suspensions, the particle-flux continuity equation incorporating a hindered-settling function is used to directly calculate a_0^*/a^* for a given distribution and initial total concentration as a function of the local particle concentration in the interface; the results, which are independent of the settling time, are shown in figure 10 for particles of type 1. Since this method for determining the size correction ratio neglects hydrodynamic diffusion, it is not rigorous. Fortunately, the resulting error is expected to be

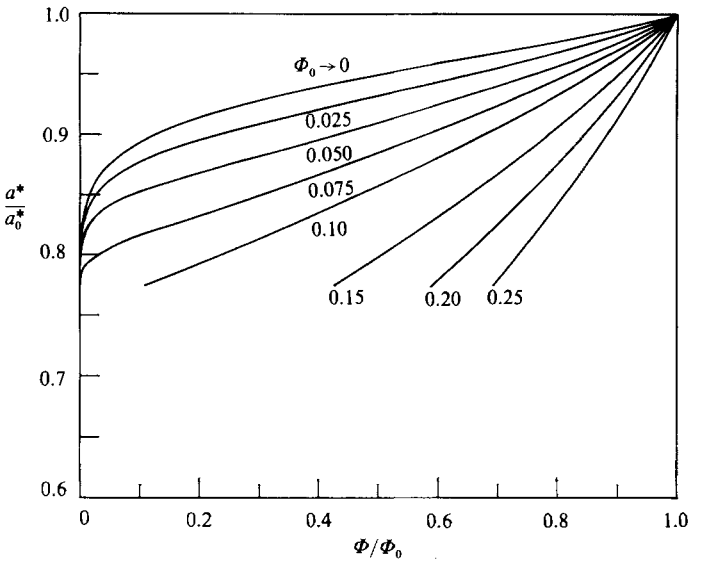

FIGURE 10. Ratio of area-averaged particle radius for a given layer in the interface to that in the initial suspension as a function of the total local concentration for $\sigma/a = 0.057$ and several values of Φ_0.

negligible. In fact, leaving the correction factor out completely leads to at most a 2% error in determining the hindered-settling velocities from the light-intensity data obtained in our experiments.

The entire sigmoidal-shaped transmitted-light-intensity curve may be analysed by the method described above to give rather complete information on the particle concentration versus time profile within the interface as it sediments past the light beam. For the present purposes, we are most interested in the vertical thickness of the sedimenting interface, and therefore a precise definition of this quantity is needed. Since the experimental method determines the particle concentration at a fixed sedimentation distance, h, as a function of time, rather than at a fixed time as a function of distance, a convenient definition of the interface thickness is given by (3.1) with t replaced by $t_{\frac{1}{2}}$:

$$\delta = (u_{\frac{3}{4}} - u_{\frac{1}{4}})\, t_{\frac{1}{2}}. \tag{4.4}$$

The settling times at which the isoconcentration planes within the interface where $\Phi/\Phi_0 = \frac{1}{4}, \frac{1}{2}$, and $\frac{3}{4}$, respectively, reach the location of the light beam are denoted by $t_{\frac{1}{4}}$, $t_{\frac{1}{2}}$, and $t_{\frac{3}{4}}$ and may be determined directly from (3.3) and the transmitted-light-intensity data. The corresponding first, second, and third quartile interface velocities are, respectively, $u_{\frac{1}{4}} \equiv h/t_{\frac{1}{4}}$, $u_{\frac{1}{2}} \equiv h/t_{\frac{1}{2}}$, and $u_{\frac{3}{4}} \equiv h/t_{\frac{3}{4}}$. Equation (3.2) for the relative quartile interface thickness is then recovered by dividing both sides of (4.4) by the settling distance, h. Note that if the three quartile velocities were constant, then the interface thickness would increase linearly with the settling distance. This is expected to be the case when the interface spreading is solely due to polydispersity in the settling velocities of individual particles, but not when particle–particle interactions lead to a diffusive spreading of the interface.

5. Results of experiments

Typical raw transmitted light intensity versus time data are shown in figure 11 for a suspension of the $-100+140$ mesh spheres (type 2) at a total initial concentration of $\Phi_0 = 0.05$ for each of four different measurement depths. There are two features of these curves that we note here. One is that they become less steep as h increases, indicative of the spreading of the interface as the sedimentation proceeds. The second is that the sigmoidal portion of each curve is less steep, in general, for times less than the time at which the middle of the interface passes the beam than for times greater than this. This indicates that the lower portion of the interface spreads more than the upper portion of the interface, an interesting feature that will be discussed more fully in §6.

5.1. *Median velocity of the interface*

Although our primary interest in this work is the spreading of the interface at the top of a sedimenting suspension, the experimental data may also be used to determine the median interface velocity in order to provide useful information on the hindered settling behaviour of a suspension. The interface median velocity, $u_{\frac{1}{2}} = h/t_{\frac{1}{2}}$, is the average velocity of the isoconcentration plane within the interface where $\Phi/\Phi_0 = \frac{1}{2}$ as it falls over the distance h. In figure 12, this velocity is made dimensionless with $u_{\frac{1}{2},0}$ and plotted versus the total initial particle volume fraction. Each data point represents the mean of all experiments performed at the given concentration. Also shown in this figure are predictions from the complete polydisperse theory of §§2 and 3 using Batchelor's theory for the hindered-settling function as given by (2.6) and also using the common empirical hindered-settling functions given by (2.7) and (2.9).

As noted previously, the theoretical predictions for the dimensionless median interface velocity do not vary significantly with the degree of polydispersity in particle sizes. The theoretical results for the two particle distributions shown in figure 12 coincide within 1%, and so only a single curve is shown for each hindered settling function. This is true even for the dashed curve which was generated using sedimentation coefficients in (2.6) that depend on the local size distribution of particles. For the more narrow particle size distribution (type 1), S_{ij} values predicted by Batchelor & Wen (1982) vary from -6.0 to -5.2 for particle sizes between plus and minus one standard deviation about the mean, whereas these coefficients for the broader distribution (type 2) vary from -6.3 to -5.0. Since these ranges are relatively small and centred on the value of $S_{ij} = -5.6$ appropriate for a nearly monodisperse suspension, it is not surprising that the results for the two size distributions are nearly identical. This justifies our approximation of using a correlation based only on the total local particle concentration, at least for the size ranges used in the experiments reported here. The greater problem is that (2.6) is restricted to dilute suspension. It is reasonably accurate for $\Phi_0 \leqslant 0.05$, but grossly underpredicts the median settling velocity for $\Phi_0 \geqslant 0.10$.

For $\Phi_0 \leqslant 0.01$, the decrease in the measured values of $u_{\frac{1}{2}}$ with increasing Φ_0 is greater than that predicted by (2.7), which has the form $u_{\frac{1}{2}} \sim u_{\frac{1}{2},0}(1-5\Phi_0)$ in the dilute limit, but it is less than that predicted by (2.9), which has the form $u_{\frac{1}{2}} \sim u_{\frac{1}{2},0}(1-\Phi_0^{\frac{1}{3}})$ in the dilute limit. For $0.01 \leqslant \Phi_0 \leqslant 0.15$, (2.7) and (2.9) give predictions that are of similar shape, except that the hindered-settling velocities predicted using (2.9) are approximately 20% less than those using (2.7). The experimental data follow the trend of these correlations and lie in between them. Note that the dilute-limit settling velocity, $u_{\frac{1}{2},0}$, was calculated from (2.5) for the median particle size and has an

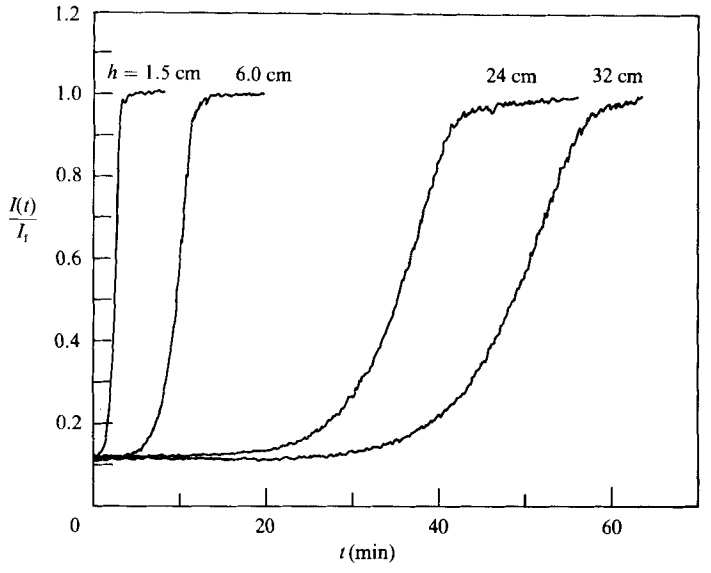

FIGURE 11. Raw transmitted light intensity versus time data for particles of type 2 at $\Phi_0 = 0.05$ and $h = 1.5$, 6.0, 24, and 32 cm.

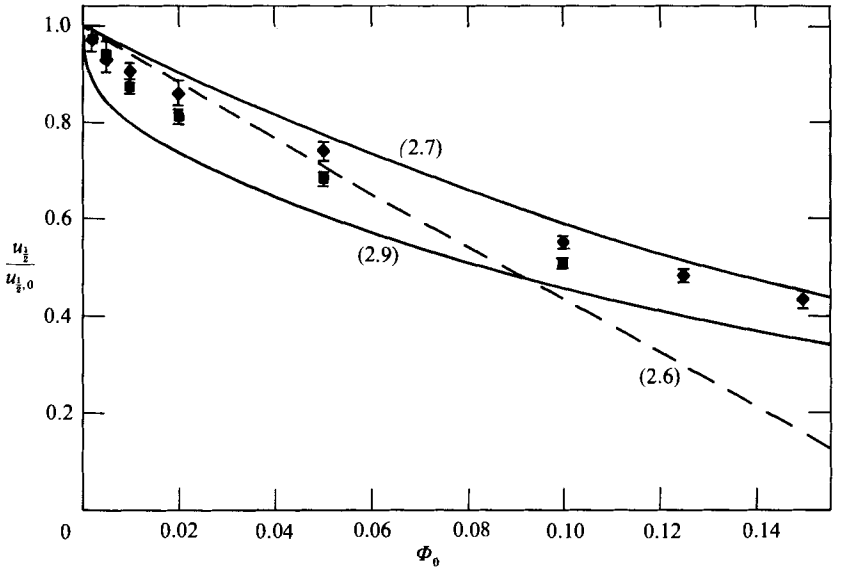

FIGURE 12. Median settling velocity data for particles of (■) type 1 and (◆) type 2. The error bars represent plus and minus one standard deviation about the mean. Also shown are the predictions of the polydisperse theory using (2.6), (2.7) and (2.9) for hindered-settling functions.

uncertainty of at least 5% due to uncertainties in the measured fluid and particle properties.

5.2. *Quartile thickness of the interface*

In addition to the median velocity, the first and third quartile velocities of the interface were calculated from the light-extinction data for each of the over 200 sedimentation experiments performed. These were then used in (4.4) to determine

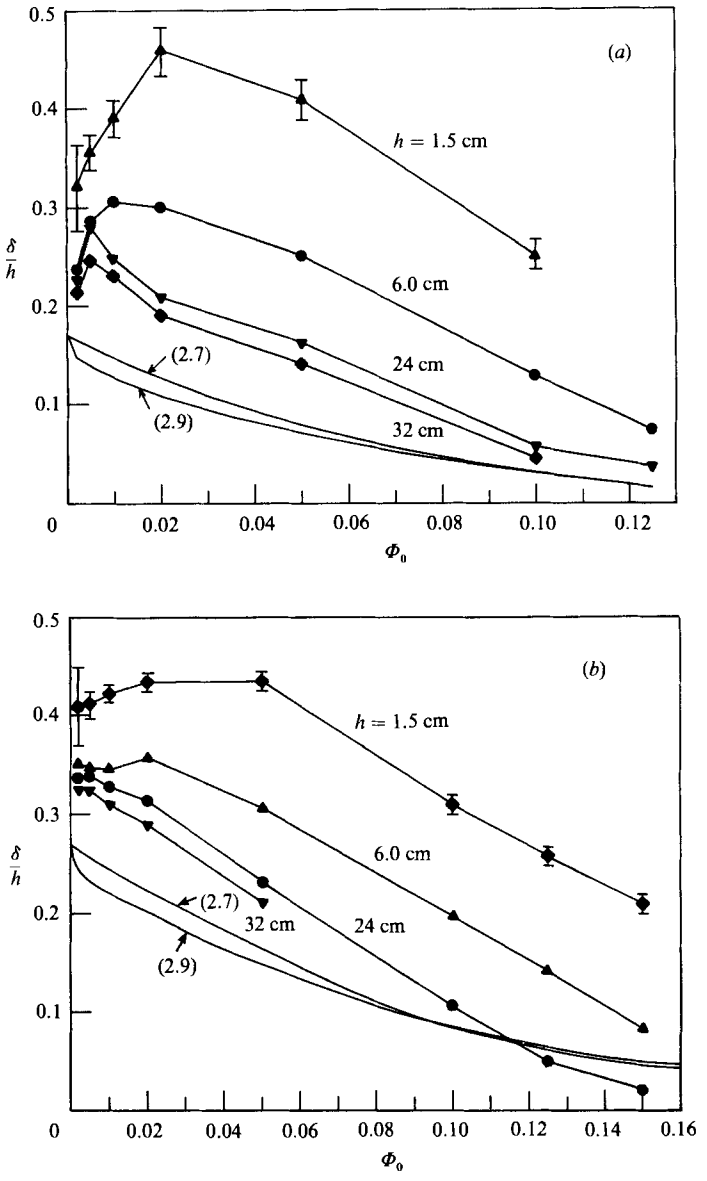

FIGURE 13. Relative quartile interface-thickness data versus concentration at four different settling depths for particles of (*a*) type 1 and (*b*) type 2. The lower curves are the prediction of the polydisperse theory using (2.7) and (2.9) for hindered-settling functions.

the quartile interface thickness, δ. In figure 13, the resulting values for the relative quartile thickness, δ/h, are shown. The data points represent mean values for the repeated experiments, and the error bars on the '$h = 1.5$ cm' curves represent plus and minus one standard deviation about the mean. In general, the error was found to be smaller for the larger values of h. Also plotted in figure 13, as the lower curves, are the values of δ/h predicted using the theory of §2. This theory, which includes polydispersity and hindered settling but not diffusion, predicts that δ/h is independent of h and decreases with increasing Φ_0 owing to the self-sharpening effect of hindered settling. Predictions using (2.6) for the hindered-settling function are

similar to those shown using (2.7) and (2.9) for dilute suspensions. When $\Phi_0 \geqslant 0.08$, the predictions using (2.6) fall below the others because of the greater hindered settling and self-sharpening given by (2.6).

The measured values of δ/h shown in figure 13 are appreciably larger than those predicted by the theory in §2. We hypothesize that the additional spreading is due to the effects of hydrodynamic diffusion. Evidence supporting this hypothesis is given in §6. The additional spreading of the interface is greatest near the top of the sedimentation vessel, and is smaller for larger values of h. This is because the vertical concentration gradients, which the diffusive flux is proportional to, are highest when the interface is near the top of the vessel and they become smaller as the interface falls and broadens.

The local maxima observed in the δ/h versus Φ_0 curves suggest that the effect of diffusion in broadening the interface increases as the particle volume fraction is increased from the dilute limit. At the same time, the self-sharpening effect of hindered settling increases, until, at a particle concentration of a few percent by volume, the competing effects balance and a maximum interface thickness is observed. For greater concentrations, the self-sharpening effect of hindered settling is stronger than the broadening one of diffusion, and the interface thickness decreases with increasing total concentration. It is also plausible that the hydrodynamic diffusivity decreases at high particle concentrations owing to the tight arrangement preventing a given particle from having significant motion relative to its neighbours, although it seems likely that this would occur at higher solids volume fractions than reported here.

6. Estimates of hydrodynamic diffusivity from interface-spreading data

In this section, we analyse the interface-spreading data in order to show that the observed spreading in excess of that expected from polydispersity and hindered-settling effects alone may be described, at least approximately, by a diffusion process. This is then used to infer information on the self-induced hydrodynamic diffusivity.

The thickness of the interface arising from the convective process associated with the distribution in particle sizes is expected to increase in proportion to the settling distance, whereas the thickness of the interface arising from a diffusional process associated with velocity fluctuations is expected to increase in proportion to the square root of the settling distance. Therefore, in figure 14, the data of figure 13(*a*) for $\Phi_0 = 0.02$ are recast in a plot of δ versus h and $h^{\frac{1}{2}}$. From this, it is seen that δ does not increase linearly with either h or $h^{\frac{1}{2}}$. Although it is expected that a diffusional spreading mechanism is dominant when the interface is near the top of the vessel, where the concentration gradient is large, and that the convective spreading mechanism of polydispersity is dominant when the interface has fallen to near the bottom of the vessel, where the concentration gradient is smaller, both of these mechanisms are important for most of the length the vessel used in our experiments. Unfortunately, the finite height of the light slit prevented us from obtaining accurate data for $h < 1.5$ cm, and the finite depth of the vessel prevented us from obtaining data for $h > 32$ cm.

In order to see whether the observed spreading in excess of that expected from the effects of polydispersity and hindered settling alone may be described as a diffusion process, the quantity δ-δ_p was calculated and then plotted versus $h^{\frac{1}{2}}$ in figure 14. Here, $\delta_p = 0.12h$ is the predicted interface thickness due to polydispersity and

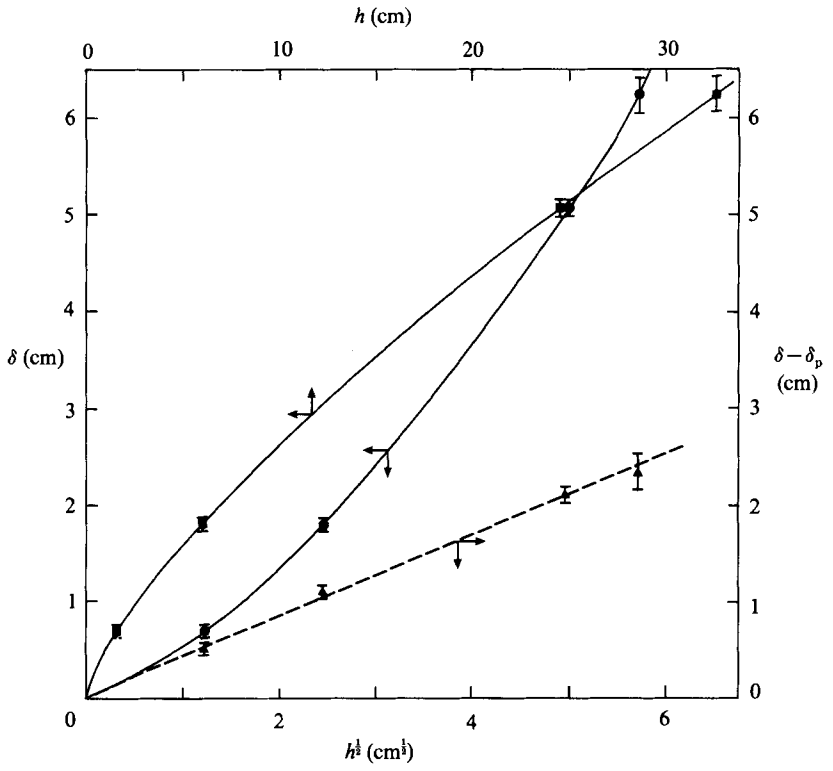

FIGURE 14. The measured dependence of the quartile interface thickness on the settling distance for particles of type 1 at $\Phi_0 = 0.02$. Also shown as the dashed curve is $\delta - \delta_p$ versus $h^{\frac{1}{2}}$, where δ is the measured interface thickness, and δ_p is the predicted interface thickness in the absence of diffusion.

hindered settling effects alone, as may be calculated from the theory of §2 using (3.2). Since the data plotted in this fashion lie approximately on a straight line through the origin, they suggest that additional spreading may indeed be described at least approximately, as a diffusion process.

An estimate of the self-induced hydrodynamic diffusivity may be made from the observed rate of spreading of the interface. The one-dimensional convective–diffusion equation with constant diffusivity D and constant median settling velocity $u_{\frac{1}{2}}$ yields the well-known solution: $\Phi/\Phi_0 = F(y)$, where $F(y)$ is the cumulative distribution function of a standardized normal random variable, and $y \equiv (h - u_{\frac{1}{2}}t)/(Dt)^{\frac{1}{2}}$. Using the definition given by (4.4) for the quartile interface thickness, along with a probability table for the function $F(y)$, this solution yields:

$$\delta_d = 1.35(Dh/u_{\frac{1}{2}})^{\frac{1}{2}}, \tag{6.1}$$

with a relative error of $O(D/u_{\frac{1}{2}}h)$. Since, in general, D and $u_{\frac{1}{2}}$ are functions of the local volume fraction Φ, which varies throughout the interface, their values in (6.1) must be interpreted as average or effective values for the interface.

The subscript d on the quartile interface thickness given by (6.1) is to emphasize that this result is for spreading due to diffusion and not polydispersity. For a suspension of spheres of radius a settling at a median hindered settling velocity $u_{\frac{1}{2}}$ in a large container at low Reynolds number and large Péclet number, there are no

other independent length or velocity scales, and so the self-induced hydrodynamic diffusivity must scale as

$$D = a u_{\frac{1}{2}} \hat{D}. \tag{6.2}$$

The dimensionless diffusivity $\hat{D}$ is a function only of the local particle volume fraction Φ. Note that we have chosen to scale the diffusivity with the median hindered settling velocity $u_{\frac{1}{2}}$ rather than the median Stokes velocity $u_{\frac{1}{2},0}$.

In order to use (6.1) and (6.2) to find the unknown dimensionless diffusivity $\hat{D}$, the spreading due to diffusion, δ_d, must be obtained from the experimental data as a function of the settling distance h. Motivated by the results shown in figure 14, which are typical of the data, the diffusive spreading is tentatively considered to be approximately equal to the measured interface spreading in excess of the theoretical predictions for polydispersity and hindered setting acting alone, i.e. $\delta_d \approx \delta - \delta_p$. Along with (6.1) and (6.2), this yields

$$\frac{\delta - \delta_p}{h} \approx 1.35 \left(\frac{\hat{D} a}{h} \right)^{\frac{1}{2}}. \tag{6.3}$$

This model must be regarded as approximate, since there is at least some coupling between the effects of diffusion, polydispersity, and hindered settling.

Equation (6.3) suggests that a plot of δ/h versus $(a/h)^{\frac{1}{2}}$ should yield a straight line with slope $1.35\hat{D}^{\frac{1}{2}}$ and intercept δ_p/h. Such a plot is shown in figure 15 using the data from figure 13(*a*) for $\Phi_0 = 0.01$ and for $\Phi_0 = 0.05$. In each case, a straight line fits the data well, adding further justification for the chosen approximate method for interpreting the data. The slope of the line for $\Phi_0 = 0.05$ is higher than that for $\Phi_0 = 0.01$, indicating an increase of the self-induced hydrodynamic diffusivity with concentration, whereas the intercept is lower for $\Phi_0 = 0.05$ than for $\Phi_0 = 0.01$, indicating a reduction of the spreading of the interface due to polydispersity with an increase in concentration because of the self-sharpening effect of hindered settling.

The slope and intercept from linear regression of the δ/h versus $(a/h)^{\frac{1}{2}}$ experimental data for each initial concentration in figure 13 are given in table 1. The intercepts are in reasonable agreement with the predicted values of δ_p/h, except that they are somewhat high for small Φ_0 and then become too low for $\Phi_0 > 0.05$. The slopes for particles of type 2 are slightly lower than those for particles of type 1, and significantly lower when $\Phi_0 = 0.02$, but the two exhibit the same trends for the diffusivity, as shown in figure 16. The inferred value of $\hat{D}$ is between one and two for the smallest concentrations investigated, increases very rapidly with increasing concentration until reaching a value between 10 and 15 for particle concentrations of a few percent by volume, and then levels off or declines slightly as the particle concentration is increased further. Table 1 and figure 16 should not be interpreted as directly giving the hydrodynamic diffusivity as a function of local concentration; instead the measured $\hat{D}$ is an effective average diffusivity for the entire interface. The fact that these diffusivities for particles of type 2 are lower than those for particles of type 1 indicates that relative particle motion due to polydispersity is not the dominant source of hydrodynamic interactions and diffusion. In fact, it is plausible that the polydispersity actually reduces the self-induced hydrodynamic diffusivity for dilute suspensions because the spread in individual particle settling velocities reduces the correlation time for particle encounters.

Finally, we return to our earlier observation that the spreading is not symmetric about the isoconcentration plane where $\Phi/\Phi_0 = \frac{1}{2}$, but that the lower portion of the interface spreads at a greater rate than does the upper portion of the interface (see

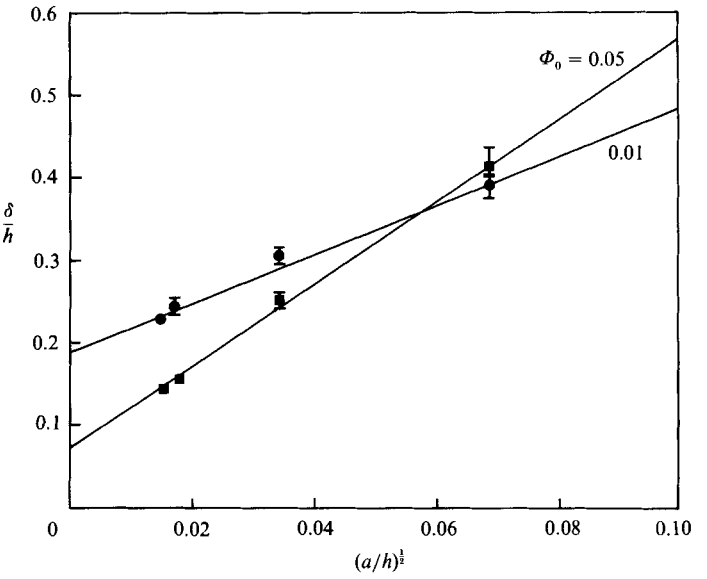

FIGURE 15. Relative quartile interface-thickness data versus $(a/h)^{\frac{1}{2}}$ for particles of type 1 at $\Phi_0 = 0.01$ and $\Phi_0 = 0.05$.

Φ_0	Particle type	Slope $(1.35\hat{D}^{\frac{1}{2}})$	$D(\mathrm{cm}^2/\mathrm{s})$	$u_{\frac{1}{2}}$ (cm/s)	Intercept (δ_p/h)	Theory (δ_p/h)
0.002	1	1.7 ± 0.5	2.0×10^{-4}	0.0180	0.20 ± 0.02	0.17
	2	1.6 ± 0.5	1.2×10^{-4}	0.0137	0.30 ± 0.02	0.27
0.005	1	1.8 ± 0.3	2.2×10^{-4}	0.0174	0.23 ± 0.01	0.16
	2	1.6 ± 0.3	1.2×10^{-4}	0.0131	0.30 ± 0.01	0.26
0.010	1	3.0 ± 0.3	5.6×10^{-4}	0.0162	0.19 ± 0.01	0.15
	2	2.1 ± 0.3	2.0×10^{-4}	0.0128	0.28 ± 0.01	0.25
0.020	1	5.0 ± 0.4	1.4×10^{-3}	0.0150	0.12 ± 0.02	0.12
	2	2.7 ± 0.3	3.0×10^{-4}	0.0121	0.26 ± 0.01	0.23
0.050	1	5.0 ± 0.3	1.2×10^{-3}	0.0126	0.07 ± 0.01	0.07
	2	4.4 ± 0.2	6.7×10^{-4}	0.0104	0.16 ± 0.01	0.16
0.10	1	4.4 ± 0.2	6.9×10^{-4}	0.0093	-0.02 ± 0.01	0.03
	2	4.1 ± 0.4	4.5×10^{-4}	0.0078	0.05 ± 0.02	0.08
0.125	2	4.1 ± 0.4	3.9×10^{-4}	0.0068	0.00 ± 0.02	0.06
0.15	2	4.0 ± 0.2	3.2×10^{-4}	0.0061	-0.04 ± 0.01	0.04

TABLE 1. Slopes and intercepts, along with their 90% confidence intervals, for least-squares linear regression of δ/h versus $(a/h)^{\frac{1}{2}}$ data. Also shown are the measured values of the median hindered-settling velocities and hydrodynamic diffusivities, and the predicted values of δ_p/h from the diffusionless theory.

figure 11). This is quantified in figure 17 where the measured quartile interface-thickness ratio $\delta_{\frac{3}{4}}/\delta_{\frac{1}{4}}$ is plotted versus $(a/h)^{\frac{1}{2}}$ for particles of type 1 at $\Phi_0 = 0.02$. The first quartile and third quartile interface thickness are defined, respectively, as

$$\delta_{\frac{1}{4}} \equiv (u_{\frac{1}{2}} - u_{\frac{1}{4}})\, t_{\frac{1}{2}}, \tag{6.4}$$

$$\delta_{\frac{3}{4}} \equiv (u_{\frac{3}{4}} - u_{\frac{1}{2}})\, t_{\frac{1}{2}}. \tag{6.5}$$

We expect that there are two major reasons for the observed $\delta_{\frac{3}{4}} > \delta_{\frac{1}{4}}$. One is the concentration buildup of the smaller particles in the upper layers of the interface due

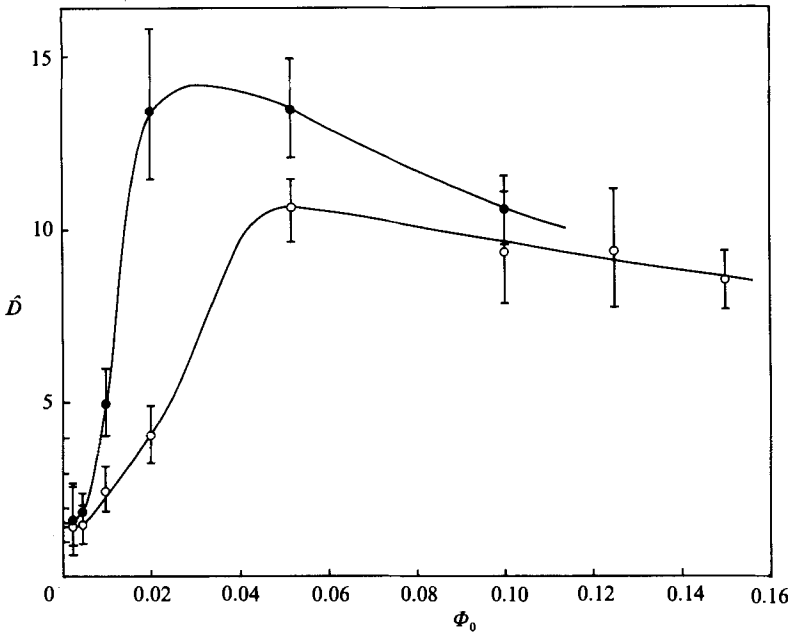

FIGURE 16. Effective value of the self-induced hydrodynamic diffusivity for the spreading interface versus particle volume fraction in the bulk suspension for particles of type 1 (●) and type 2 (○).

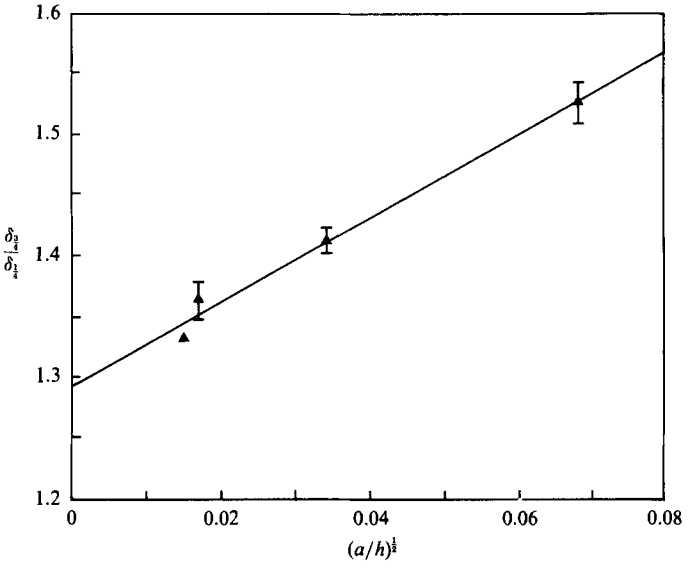

FIGURE 17. The measured quartile interface-thickness ratio for particles of type 1 at $\Phi_0 = 0.02$.

to hindered settling and particle-flux continuity requirements, as discussed in §3. As was seen in figure 5, this leads to a relatively small spread in settling velocities in the upper portion of the interface compared with that in the lower portion of the interface. The predicted value of $\delta_{\frac{3}{4}}/\delta_{\frac{1}{4}}$ for $\Phi_0 = 0.02$ in the absence of diffusion is 1.3, in good agreement with the intercept of the data regression shown in figure 17. Second, it is expected that the self-induced hydrodynamic diffusivity has a higher value near the bottom of the interface than near the top of the interface since the

average particle concentration, size and settling velocity are higher in the lower layers of the interface. This gives a greater asymmetry in the spreading for smaller settling distances.

7. Concluding remarks

In this paper, the spreading of the interface at the top of a sedimenting suspension of non-Brownian particles has been examined in the light of three factors: a polydisperse distribution in particle sizes which yields a vertical interface thickness that increases in proportion to the settling distance and to the spread in particle sizes; hindered-settling effects which become increasingly important as the solids concentration is increased and which cause a self-sharpening of the interface; and a self-induced hydrodynamic diffusion process arising from fluctuations in the particle fall speeds as they interact with one another and which leads to a vertical interface thickness that increases with the square root of the settling distance. Transmitted-light-intensity measurements of the interface showed that its thickness may be much greater than that expected from the small degree of polydispersity in the particles used, especially for short settling distances. The measured interface thickness in excess of that predicted from a diffusionless theory accounting for polydispersity and hindered settling was found to increase approximately in proportion to the square root of the settling distance, as is characteristic of diffusional processes. These data were used to estimate the magnitude and concentration dependence of the self-induced hydrodynamic diffusivity. Using the resulting values along with (3.4) in (6.3) shows that the ratio of spreading due to hydrodynamic diffusion to that due to polydispersity for non-concentrated suspensions is approximately $(a/h)^{\frac{1}{2}}/(\sigma/a)$. Over a wide range of settling distances and particle size distributions, both of these spreading mechanisms are important.

The self-induced hydrodynamic diffusivities reported in table1 and figure 16 must be regarded as approximate, both because of the moderate scatter in the data and because of the approximate nature of the data analysis. This is especially true for the higher concentrations because hindered settling may be expected to reduce the spreading due to diffusion; hindered settling was not accounted for in the estimation of the diffusivity other than by reducing the constant value used for the median settling speed, $u_{\frac{1}{2}}$. Also, the inferred diffusivities depend most strongly on the data for small h. Since particles must fall far enough to undergo several encounters with other particles before their fluctuations may be described as diffusive, there may be some inaccuracies in the data interpretation for small h and small Φ_0. In particular, some initial convective spreading of the interface would be expected even for a monodisperse suspension, since particles that are close to one or more other particles fall faster than the mean and leave the isolated particles behind. This phenomenon of clusters of particles falling more rapidly than single particles and leaving behind a depleted, fuzzy interface containing slower-settling isolated particles has been described previously in the sedimentation literature (Tory & Pickard 1986). Also, since it is difficult to stir the suspension near the top of the vessel without entraining air bubbles, the initial conditions may depart from the uniform suspension assumed in the model. However, this is not expected to be an important factor, since extrapolation of the data to the top of the vessel ($h = 0$) shows that the initial interface thickness is negligible compared with the excess interface thickness observed at the measured depths (see figure 14).

In spite of the approximate nature of our analysis, we feel that the present findings

are significant because they show that self-induced hydrodynamic diffusion is a surprisingly strong phenomenon. For the suspensions described in this paper, typical dimensional hydrodynamic diffusivities are on the order of 10^{-3} cm^2/s, whereas the Brownian diffusivities are only on the order of 10^{-13} cm^2/s. The hydrodynamic diffusivities reported in this paper should be regarded as average quantities for the interface as a whole rather than as local values referring to a specific particle volume fraction. Also, since a particle concentration gradient is present in the interface, these diffusivities are collective (down-gradient) diffusivities which may be different from the coefficient of self-diffusion which would be observed by following an individual particle in the interior of a homogeneous suspension. Experiments to measure the latter have recently been reported by Ham & Homsy (1988). Clearly, further work involving more definitive experiments and theory on self-induced hydrodynamic diffusion is needed.

This research was supported by the National Science Foundation under Grant No. CBT-8451014 and by the Exxon Chemical Company. Several discussions with Professor G. K. Batchelor during visits by R. H. Davis to the Department of Applied Mathematics and Theoretical Physics at the University of Cambridge were also instrumental in the development of this work.

REFERENCES

Barnea, E. & Mizrahi, J. 1973 A generalized approach to the fluid dynamics of particulate systems: Part 1. General correlation for fluidization and sedimentation in solid multiparticle systems. *Chem. Engng J.* **5**, 171–189.

Batchelor, G. K. 1982 Sedimentation in a dilute polydisperse system of interacting spheres. Part 1. General theory. *J. Fluid Mech.* **119**, 379–408.

Batchelor, G. K. & Janse van Rensberg, R. W. 1986 Structure formation in bidisperse sedimentation. *J. Fluid Mech.* **166**, 379–407.

Batchelor, G. K. & Wen, C. S. 1982 Sedimentation in a dilute polydisperse system of interacting spheres. Part 2. Numerical results. *J. Fluid Mech.* **124**, 495–528.

Davis, R. H. & Acrivos, A. 1985 Sedimentation of noncolloidal particles at low Reynolds numbers. *Ann. Rev. Fluid Mech.* **17**, 91–118.

Davis, R. H. & Birdsell, K. H. 1988 Hindered settling of semi-dilute monodisperse and polydisperse suspensions. *AIChE J.* **34**, 123–129.

Davis, R. H., Herbolzheimer, E. & Acrivos, A. 1982 The sedimentation of polydisperse suspensions in vessels having inclined walls. *Intl J. Multiphase Flow* **8**, 571–585.

Durlofsky, L., Brady, J. F. & Bossis, G. 1987 Dynamic simulation of hydrodynamically interacting spheres. *J. Fluid Mech.* **180**, 21–49.

Eckstein, E. C., Bailey, D. G. & Shapiro, A. H. 1977 Self-diffusion of particles in shear flow of a suspension. *J. Fluid Mech.* **79**, 191–208.

Greenspan, H. P. & Ungarish, M. 1982 On hindered settling of particles of different sizes. *Intl J. Multiphase Flow* **8**, 587–604.

Ham, J. M. & Momsy, G. M. 1988 Hindered settling and hydrodynamic dispersion in quiescent sedimenting suspensions. *Intl J. Multiphase Flow* (in press).

Hassen, M. A. 1987 Interface spreading in polydisperse sedimentation. M.S. Thesis, University of Colorado, Boulder, Colorado.

Herdan, G. 1960 *Small Particle Statistics*, 2nd edn. Academic.

Leighton, D. & Acrivos, A. 1987*a* Measurement of the shear-induced coefficient of self-diffusion in concentrated suspensions of solid spheres. *J. Fluid Mech.* **177**, 109–131.

Leighton, D. & Acrivos, A. 1987*b* The shear induced migration of particles in concentrated suspensions. *J. Fluid Mech.* **181**, 415–439.

RICHARDSON, J. F. & ZAKI, W. N. 1954 Sedimentation and fluidisation: Part 1. *Trans. Instn Chem. Engrs* **32**, 35–52.

SMITH, T. N. 1966 The sedimentation of particles having a dispersion of sizes. *Trans. Instn Chem. Engrs* **44**, 153–157.

TORY, E. M. & PICKARD, D. K. 1986 Experimental evidence for a stochastic approach to sedimentation. *Proc. Engng Foundation Conf. on Flocculation, Sedimentation and Consolidation, Sea Island, Georgia, Jan. 27–Feb. 1, 1985* (ed. B. M. Moudgil and P. Somasundaran), pp. 297–306. AIChE.